RSC Advances

PAPER

View Article Online
View Journal | View Issue



Cite this: *RSC Adv.*, 2025, **15**, 14778

# The enhanced ultrafast dissociation of *meso*-hydrogen of bis(indolyl)methane derivatives under acidic conditions†

Vikas Kumar Jha,[a] Sunil Kumar Patel,[a] Devarapalli Chenna Rao,[b] Kovuru Gopalaiah[b] and E. Siva Subramaniam Iyer *[a]

Received 22nd March 2025
Accepted 29th April 2025

DOI: 10.1039/d5ra02015h

rsc.li/rsc-advances

Bis(indolyl)methane (BIM) derivatives are an important class of molecules that have shown vivid applications. The photo dynamics of BIM derivatives has been studied through ultrafast spectroscopy. It has been observed that the acidic medium plays a vital role in governing the spectral characteristics of BIMs, imputing to the ambivalent nature of BIMs under acidic conditions. We noticed that the dissociation of *meso*-hydrogen is enhanced under acidic conditions, while no such enhancement is observed under alkaline and neutral conditions. We further perceived that the dissociation of *meso*-hydrogen takes precedence over the dissociation of N–H bonds, even in an acidic medium. Quantum chemical calculations support the experimental observations. Although the functionalisation with electron-withdrawing or electron-donating groups seems to affect photophysical properties such as spectral shift, quantum yield, *etc.*, tuning the acidic medium plays a significant role.



## Introduction

The design and development of sensitive chromophores that respond to changes in microenvironments have gained significant attention over the years.[1–4] Central to these innovative systems is the intriguing concept of modifying the electronic structure of chromophores, which are crucial for targeted applications. Such modifications may be prompted by various factors, including acid–base interactions, intramolecular charge transfer, hydrogen bonding, molecular aggregation, *etc.* Highly conjugated molecular systems are particularly advantageous due to their ability to absorb and emit in the visible spectrum, making them attractive for various applications. Notably, heterocyclic compounds emerge as promising candidates as they exhibit polychromism under specific conditions owing to their diverse inter- and intra-molecular interactions.

A particularly noteworthy structural motif present in both natural and synthetic compounds is the indole scaffold, which demonstrates exceptional versatility and potential.[2–9] Indole derivatives, particularly bis(indolyl)methanes (BIMs), are integral to numerous bioactive molecules, fine chemicals, pharmaceuticals, agrochemicals, and functional materials.[10–18] These compounds exhibit a broad spectrum of biological activities—including anti-inflammatory, antibacterial, anti-infective, and anticancer properties—while also presenting valuable opportunities for research and development.[4,19–24] The bioavailability and reactivity of BIMs can be affected by the intermolecular interactions between the molecules and cellular components. This has inspired many dedicated researchers globally, including us, to concentrate on the synthesis of BIMs and their derivatives.[3,25–32] Furthermore, derivatives of BIMs are being actively studied, showcasing tuneable properties that enhance their potential applications in various fields. For example, the oxidised derivatives of BIMs are used for developing chemical sensors.[33,34] The aggregation-disaggregation induced photophysical properties can be tuned by altering the microenvironment.[35–37] Therefore, understanding the molecular design strategies and their inter-relation with photophysical properties as well as molecular excited state dynamics depending on the solvent environment of BIM molecules become important. The future of this research area is promising and offering numerous opportunities for discovery and advancement.[38–40]

It would be beneficial to delve into the photophysical properties of BIM derivatives, particularly focusing on the excited state characteristics that influence their interactions. The BIMs exhibit a prominent absorption band in the UV range (220 nm to 290 nm), attributed to an allowed ππ* intra-ligand transition. In the oxidised BIMs, an additional low-energy band appears between 490–530 nm, corresponding to intra-ligand or ligand-to-ligand charge transfer transitions.[33,34] These assignments arise from observations that when aryl groups substituted on

[a]*School of Chemical and Materials Science, Indian Institute of Technology Goa, Farmagudi, Ponda, Goa 403 401, India. E-mail: vikas19251104@iitgoa.ac.in; sunil21251103@iitgoa.ac.in; essiyer@iitgoa.ac.in*

[b]*Department of Chemistry, University of Delhi, Delhi 110 007, India. E-mail: dchennarao@yahoo.co.in; gopal@chemistry.du.ac.in*

† Electronic supplementary information (ESI) available. See DOI: https://doi.org/10.1039/d5ra02015h


Fig. 1 Bis(indolyl)methane derivatives used in this study.

the bridging methyl carbon contain electron-withdrawing heteroatoms, the excitation to a higher energy band generates an extra emission peak centred at 560 nm, which is associated with the charge transfer state.[41,42] Theoretical calculations utilising time-dependent DFT confirm the existence of two sets of absorption bands. The HOMO and LUMO molecular orbitals are primarily localised on the indole and *meso*-substituted aryl groups, respectively, and contribute to the high-energy absorption profile.[39,43–45]

Phenyl(bisinodyl)methane (BIM **I**, Fig. 1) displays aggregate formation in aqueous environments. However, as polarity diminishes and relative hydrophobic microenvironment enhances, *e.g.* when confined in micellar systems, a disaggregation phenomenon occurs. Notably, the emission intensifies with increasing charge on the surfactant head groups. A similar confinement effect is noted in β-cyclodextrin (β-CD), where an increase in emission intensity is attributed to the disaggregation process.[35–37]

In the context of BIM derivatives, reversible deprotonation of the –NH bond can occur. Given that indole has a p$K_a$ exceeding 16, conventional protonation of the –NH bond is unlikely. However, under specific conditions, the bridging carbon's tendency to lose the *meso* proton and form a coloured compound invites further investigation into the dynamics of these molecules. This study presents the ultrafast excited-state dynamics of three distinct aryl-substituted BIM derivatives, with their structures depicted in Fig. 1. Two derivatives feature electron-donating or electron-withdrawing substituents at the fifth position of the indole ring, while the third remains unsubstituted. We analysed the excited-state dynamics across varying acidity levels for these compounds, as well as their behaviour in sodium dodecyl sulphate (SDS) micellar medium. Our findings highlight an increased likelihood of *meso*-H deprotonation in the excited state compared to the ground state, an effect that is amplified when steric factors induce molecular distortion. Interestingly, the absorption spectra of BIM **I** exhibit minimal sensitivity to its local environment.

## Experimental methods

The three BIM derivatives were prepared using the procedures published elsewhere and briefly described in the ESI.† [3] The stock solutions for spectral measurements were prepared by dissolving a few milligrams of the sample in 1 mL of freshly distilled methanol. For the transient absorption measurements, the stock solutions were diluted in methanol to have an OD of around 0.6 for BIM **I** ($\varepsilon$ = 16 796 $M^{-1}$ $cm^{-1}$), 0.4 for BIM **II** ($\varepsilon$ = 11 807 $M^{-1}$ $cm^{-1}$), and 0.3 for BIM **III** ($\varepsilon$ = 8825 $M^{-1}$ $cm^{-1}$), in a 2 mm path-length cell at the wavelength of excitation. The normalised absorption and fluorescence spectra are shown in Fig. S1.† The molecules exhibited linear Beer–Lambert plot even at higher concentrations (Fig. S2†). The resulting solutions were in the order of $10^{-4}$ M, with respect to the molecule of interest. In order to achieve an acidic or alkaline medium, 10 equivalents of HCl ($10^{-3}$ M), and NaOH ($10^{-3}$ M), respectively, were added to the stock solution before diluting with methanol. The photophysical parameters were studied in sodium dodecyl sulphate (SDS) micellar medium as well. The concentration of SDS was kept at 30 mM. Beyond this concentration, there was no change in the absorption or emission spectrum of the BIM derivatives. The samples were freshly prepared for each spectroscopic measurement. Steady-state absorption spectra were recorded using a JASCO V-770 UV-Vis-NIR spectrophotometer, and fluorescence emission was recorded on an Agilent Cary Spectrofluorometer. To understand the excited state dynamics of BIM derivatives, femtosecond transient absorption measurements were performed on a Helios fire transient absorption spectrometer (Ultrafast systems, USA) pumped by an Opera Solo OPA (Optical Parametric Amplifier). The OPA is pumped by a fraction of 35 fs, 5 mJ pulse centred at 800 nm produced from Astrella Amplifier (Coherent, USA) operating at 1 kHz. Another fraction of the amplified output is used for the generation of a white light probe. The transmitted probe light in the presence and absence of the pump pulse was detected on a CCD spectrograph. The pump and probe were maintained at parallel polarization with respect to each other. The samples were irradiated with a pump pulse centred at 285 nm, having pulse energy of 250 nJ at the output of OPA. A broadband White light probe (450–780 nm) was generated on a Sapphire window. The samples were stirred throughout the measurement with a magnetic stirrer. The sample integrity was checked by measuring absorption spectra at various intervals during the course of the experiment. The spectra and kinetics were analysed using Surface Xplorer V4 and Origin 2019.

The theoretical calculations were performed using GAUSSIAN 16 package.[46] The visualisation of the molecule is done by Gauss-View 6.0 molecular visualisation program. The geometries of BIM derivatives, protonated and oxidised forms were optimised using Becke's three parameters with the Lee–Yang–Parr hybrid exchange-correlation function (B3LYP) with the basis set of 6-31G (d).[47–50] The geometry optimisation for the lowest excited singlet state ($S_1$) using time-dependent DFT (TD-DFT) calculations using the same functional and basis sets. All the calculations were performed considering molecules in the gas phase.

## Results and discussions

The absorption spectra of BIM derivatives in methanol, acidic and alkaline media are shown in Fig. 2. The absorption spectra of BIM derivatives in methanolic solutions show indole-like vibronic features (Fig. S1†). This is trivial as the two indole moieties are not in conjugation with each other. However, despite lacking conjugation, the BIM spectrum is red-shifted compared to indole. This band undergoes further red shift

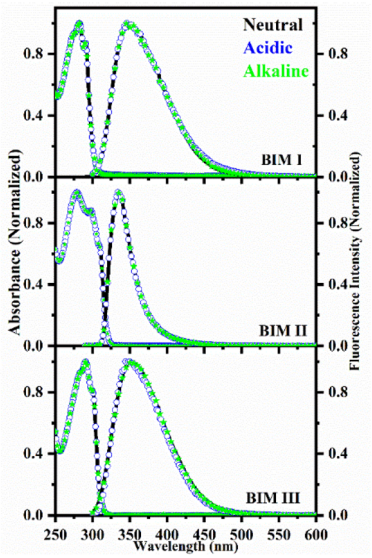


Fig. 2 Normalised Steady-state absorption and fluorescence spectra of BIM I, BIM II, and BIM III in methanol (labelled as neutral, black line), acidic (blue circles) and alkaline (green circles) methanolic medium.

upon substitution of the benzenoid ring of the indole moiety. The broadest spectra are obtained when the indole rings are substituted with electron-donating methoxy groups. This could be attributed to the lifting of degenerate electronic states similar to substituted indoles.[51,52] In BIM **II**, such resolution is possibly absent because the two indoles are not equivalent due to the bulky methoxy groups. The red shift due to halogen substitution is well known in organic molecules, and the same reason could be attributed to the chloro-substituted BIM.[41] The absorption spectra are unaffected by the addition of HCl or NaOH to the methanolic solutions of BIMs (Fig. 2). This is observed even at concentrations as high as ten equivalents of acid or alkali. Such invariance shows that the ground state is the same irrespective of the pH of the medium. The invariance of spectra and structured absorption suggest that aggregation induced effects are absent for any of the compounds.[35,36] There have been several reports which have attributed sensing properties of BIM derivatives to oxidation at *meso*-carbon or binding to ions *via* indole-NH groups.[38–40] Had those been the case, the high acidity or alkalinity used in the current experiments should have triggered any previously noticed spectral shifts. Based on our experience, such degradation was observed only upon photoexcitation and has been presented in subsequent discussions. At this stage, attention must be paid to the absorption spectrum of BIM **II**, which is broad and covers indole and the other two BIM derivatives. This suggests the possibility of the two indole rings being in different environments. Broader absorption spectra suggest more degenerate $L_a$ and $L_b$ states in the BIM derivative, and one can excite these molecules at different wavelengths to understand the dynamics of indole more clearly, which is still debatable. This study is beyond the scope of this work and will be addressed in future.

The respective fluorescence spectra of BIM **I** to **III** do not exhibit any shifts with changes in acidity of the medium,

Table 1 The stoke shift and relative quantum yield of BIM derivatives. The relative quantum yield is calculated from the OD-corrected emission spectra and compared with indole

| Name | $\lambda_{abs}^{max}$ (nm) | $\lambda_{ems}^{max}$ (nm) | $\Delta\lambda$ (nm) | Relative QY |
|---|---|---|---|---|
| Indole | 271 | 329 | 58 | 1 |
| BIM **I** | 282 | 351 | 69 | 0.15 |
| BIM **II** | 279 | 334 | 55 | 0.48 |
| BIM **III** | 291 | 352 | 61 | 0.014 |

suggestive of the same excited state for all the molecules. The relative quantum yields of the three compounds with respect to indole are tabulated in Table 1.

The emission spectra are obtained by exciting the samples at 280 nm and are corrected for absorbance effects while calculating the quantum yields. The quantum yield is maximum in the presence of the electron-donating methoxy group, whereas the chloro-derivative has the lowest quantum yield. Earlier investigations on BIM **I** have reported an enhanced emission attributed to the hindered rotations in viscous media.[35] In BIM **II**, the bulky methoxy group can cause a similar effect, consequently increasing the quantum yield. These observations are in line with the earlier reports on similar compounds.[38–40] It is worthwhile to note that the fluorescence spectrum of BIM-II is significantly narrow and remarkably resembles indole (Fig. S1†). It is proposed that indole has two excited states *viz.* $L_a$ and $L_b$, and the latter contributes to fluorescence.[53] It is possible that due to the relative orientation of the indole rings in BIM **II**, the molecules retain indole features. While in BIM **I** and BIM **III** these two states are possibly coupled resulting in broad fluorescence spectra. However, the coupling cannot be conclusively said. A significant drop in the quantum yield for BIM **III** could not just be associated with the halogen effect of chlorine, but to some other excited state process involved which cannot be concluded from steady state spectroscopy measurements alone. Earlier works on BIM **I** have reported the fluorescence lifetime of 1–1.5 ns that can go up to 3 ns in restricted environments.[36,37] An effect of solvent is also noticed. A decrease in quantum yield in aqueous solvents are ascribed to aggregation phenomena. The aggregation manifests as distinct changes to the steady state spectra accompanied by loss of vibronic structures in the absorption spectrum. In our measurements all molecules retain vibrational features thus we rule out aggregation as a cause of decreased quantum yields.

Femtosecond transient absorption spectroscopic measurements were performed to ascertain the excited-state dynamics of BIM derivatives. Equivalent experiments were carried out in neutral (prepared methanolic solution), acidic, and alkaline conditions (10 equiv.). The samples were pumped at 285 nm. During the course of measurements, the polarizations for the pump and the probe were maintained parallel with respect to each other. The kinetic traces in cross-polarized conditions yielded similar kinetic traces, hence ruling out rotational anisotropy (Fig. S3†). Under acidic conditions, the laser excitation resulted in the evolution of a new band centred at 500 nm

(Fig. S4†). Such a band was not observed in neutral and alkaline conditions. This band has already been assigned to the oxidised form of BIM derivatives.[33,34,39] The oxidised form is obtained by the loss of the *meso* hydrogen, resulting in an extended conjugation all the way from the phenyl group to the indole ring. This increased conjugation is responsible for the colour, which is used as a marker for sensor applications.[54] The absorption band in the region 450–550 nm in oxidised BIMs is assigned to the intra-ligand charge transfer.[39,55] In the case of BIM **III**, the chloro group due to its electron withdrawing nature can result in a less pronounced charge transfer state and results in blue-shifted spectra compared to BIM **I**. We suspect that the BIM derivatives should retain some of the indole-like features, and to ascertain this, experiments were performed in methanolic solutions of indole as well. Within the probed region (450 nm to 750 nm), the indole shows a strong excited state absorption which decays over a few nanoseconds. Besides this, no other unusual feature is observed (Fig. S5†). The excited state absorption (ESA) originates from a stabilised excited state. This state is formed within few picoseconds post-excitation. The sub-picosecond internal conversion reported for indole is outside the range of wavelengths probed in current investigations. The invariance in the kinetic traces raises doubt over the role of the N–H bond on the excited state dynamics of indole, as reported earlier.[56,57] It could be argued that the states are missed due to the time resolution of the experiment. However, even if this were the case, the formation of the excited state should have been affected, which does not appear to be the case. Thus, the role of N–H, if at all, could be important when indole is excited to higher energy levels with UV excitation at wavelengths less than 270 nm. The earlier experiments have also indicated the wavelength selectivity on the kinetics of the excited states when excited to higher energies.[58,59] However, in this work the samples are excited at 285 nm, which is close to the red edge of indole.

The TA spectra of BIM derivatives are dominated by excited state absorption (Fig. 3 and S6–S8†) in the entire probe range. In addition, a negative signal is observed under acidic conditions. The spectral features of absorption are similar to those of indole. This suggests the indole-like features are still retained in the molecule. The negative signals and the ESA will be discussed later, as we suspect these features come from distinctly different molecules. The decay of ESA in BIM **III** is significantly faster. The kinetic traces of indole and BIM derivatives in neutral conditions at different wavelengths are shown in Fig. 4. The kinetic traces in acidic and alkaline conditions are shown in Fig. S9.† The kinetic traces of BIM **I** are faster than indole but slower than the chloro derivative (BIM **III**). This aligns with our observation from steady-state measurements, where we have observed very low quantum yields. Thus, the excited state

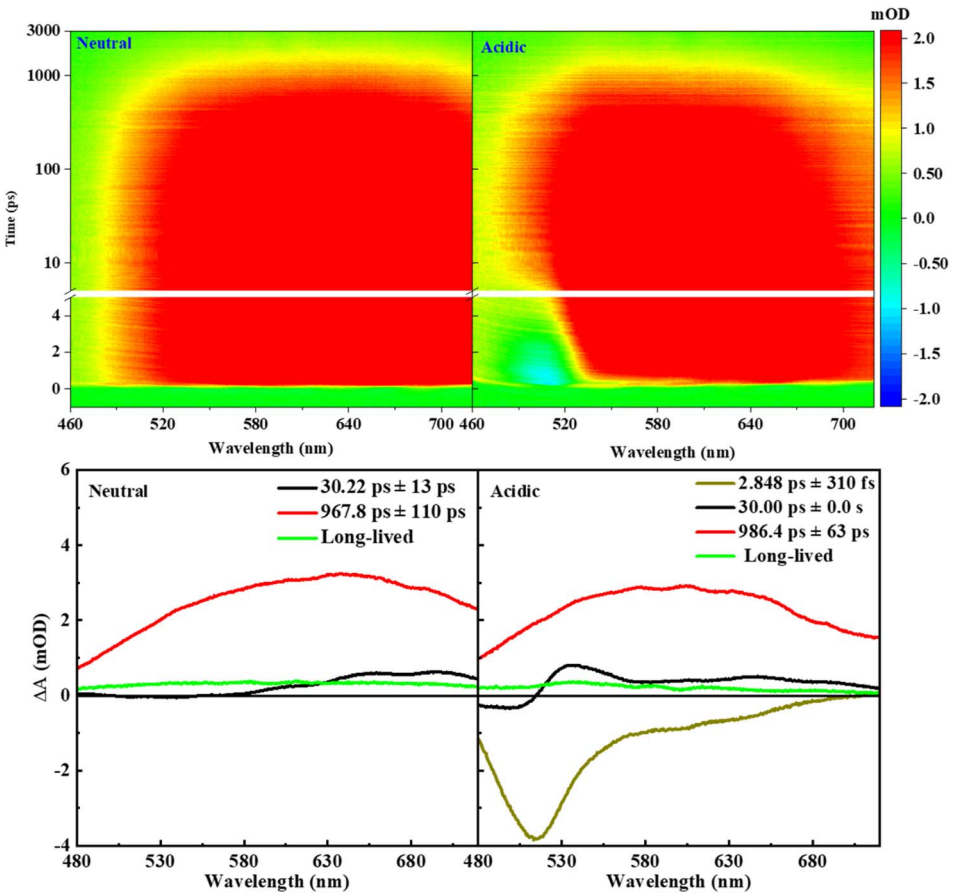


Fig. 3 TA spectra (above) and EADS (below) of BIM **I** in a neutral medium and in the presence of 10 equivalents of acid.

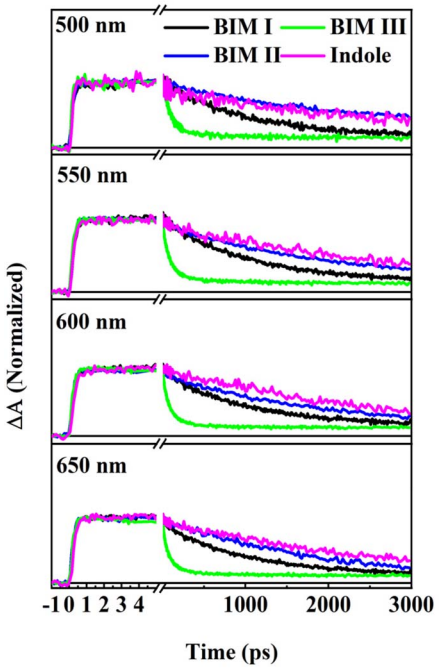


Fig. 4 Kinetic traces of BIM derivatives and indole under neutral conditions at 500 nm, 550 nm, 600 nm, and 650 nm.

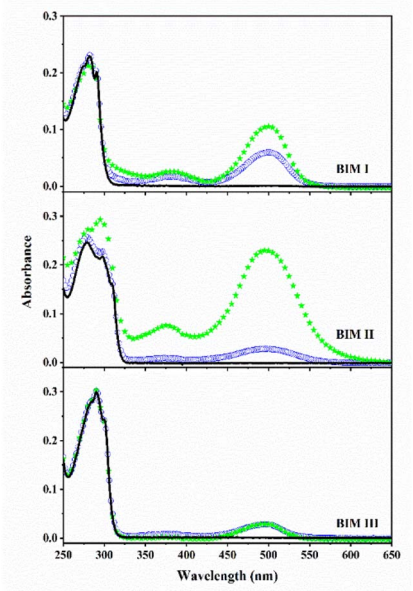


Fig. 5 Comparison of absorbance of BIMs before laser irradiation (black line) after irradiation (blue circle) and after keeping five days in ordinary light after irradiation (green star).

reached upon excitation is deactivated, which could possibly be due to hydrogen bonding in BIM-H, and the halogen effect and the intra-ligand charge transfer effects in BIM **III**. The spectral and kinetic features are similar in alkaline conditions. This is not unusual as the p$K_a$ of indole is close to 18 and not expected to ionise in the ground state to alter the spectral features. The most interesting features are noted under acidic conditions. In addition to the routine ESA, a negative signal is observed. The amplitude of the negative signal is in the order BIM **I** > BIM **III** > BIM **II**. Although the negative signal is not distinctly apparent from the TA spectra, a careful examination shows that the signals in the blue edge are weak. This suggests that the ESA and the negative signal cancel each other. The evolution-associated decay spectra obtained by global kinetic analysis clearly revealed the negative signals at 500 nm for all three molecules under acidic conditions (Fig. S6–S8†). Now, this band is observed at the same wavelength as the lowest energy absorption band of oxidised BIM. Hence, we assign this band to the bleach of the ground state of the oxidised form. Also, this band is very short-lived. The average lifetime of the negative signal is around 3 ps for BIM **I**, 5 ps for BIM **II**, and 10 ps for BIM **III** (Table ST1†). This oxidised form could be generated by deprotonation of the *meso*-H. The relative amounts of oxidised form increases with each scan. However, the extent is different. The ratio of signals corresponding to the native molecules and oxidised molecules can be a good measure of the same. The ratio of Δ$A$ at 500 nm and 550 nm at a delay of 500 fs as a function of scan number is shown in Fig. S10.† The extent of deprotonation is highest for BIM-I showing its propensity to lose the *meso* H to form the oxidised product. Under strongly acidic conditions, the only likelihood of protonation is at the N centres of the BIM derivatives. This would induce a positive charge on the indole rings, which may affect the geometry of the molecules. As a result, the molecule may acquire a different geometry upon excitation, which promotes the loss of H at the *meso* position. This would serve a dual purpose: reduce the positive charge, and acquire a more stable orientation. In the neutral and alkaline cases, we did not see any significant population giving rise to a negative signal. A short component with a lifetime of tens of picoseconds is noticed, but it contributes mainly to the build-up of the ESA. Thus, it may be attributed to the formation of low-energy excited state from a locally excited state reached by the excitation of a 285 nm pump. To ascertain photochemistry, the solutions were kept in ambient light for five days. During this period, the absorption band at 500 nm became stronger (Fig. 5). When pumped at 500 nm, the light-adapted samples resulted in the same GSB kinetics as observed with acidic samples (Fig. 6). The photochemical

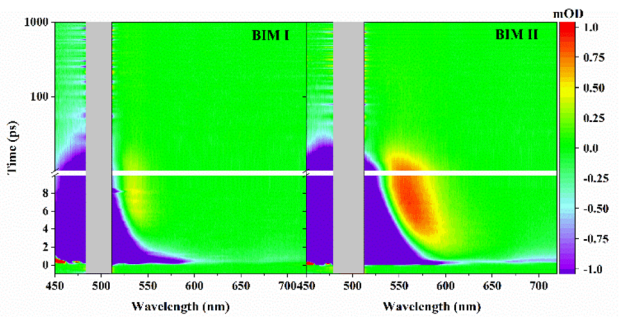


Fig. 6 The 2D plots of TA spectra with 500 nm pump excitation for BIM I and BIM II (in acidic methanol that is kept for five days in ordinary light after 285 nm excitation).

conversion with BIM-III was negligible. Hence, an equivalent experiment could not be performed with BIM-III. Based on observations so far, we conclude that the excited molecules lose the *meso* H and form the oxidised product under acidic conditions.

In order to substantiate the experimental observations, quantum chemical calculations have been carried out. The influence of solvent is not taken into consideration, although it is known that dielectric medium can affect the energy levels. Our intention is to monitor the strength of *meso* CH bond in ground and excited state, which can be estimated from gas phase calculations. The calculations were executed on native BIM derivatives, oxidised BIM derivatives, and protonated BIM derivatives where the indole nitrogen is protonated. In the oxidised molecules, we have assumed conjugation extends only to one indole and protonation is considered for the other indole moiety. A common feature of all systems is that HOMO orbitals are localised over the indole rings, while in the LUMO orbital, the electron density is shifted towards the aryl groups (Fig. S11 and S12†). This observation is in line with earlier studies on similar molecules.[60] An enhanced electron density over the bridging carbon could lose proton more quickly than the protonated nitrogen. This explains why the *meso*-H is lost to yield an oxidised product. Indubitably, we understand the protonation of indole might not be taking place in the ground state and is evident from the absorption spectra where there is no change irrespective of the medium. We have made this hypothetical system so that a reasonable understanding be developed for the process in excited states (Fig. S13 and S14†). The optimised geometries of BIMs and oxidised BIMs are shown in Fig. 7. It is worthwhile to notice that the relative orientations of the two indole rings have the nitrogen face in opposite directions in BIM **I** and BIM **III**. Upon oxidation, one of the rings rotates, and both nitrogen faces are on the same side. This trend is the opposite for BIM **II**, where in the oxidised form the nitrogen atoms continue to be on opposite sides. However, this creates increased crowding due to the bulky methoxy groups and is expected to be unfavourable. Consequently, oxidation is not favoured. This explains the decreased propensity of BIM **II** to lose the *meso* H and is reflected in our experiments, where the negative bleach band is weak. However, the molecule's tendency to lose *meso* H can be triggered by laser irradiation (Fig. 5). In the excited state, electron density on the *meso*-C increases and rotation gets hindered, hence the formation of the oxidised product becomes more feasible.

Further evidence for the formation of the oxidised product was obtained by comparing the orbital energies of the protonated, oxidised and native molecules. The energy level diagram considering the three HOMO and three LUMO levels are shown

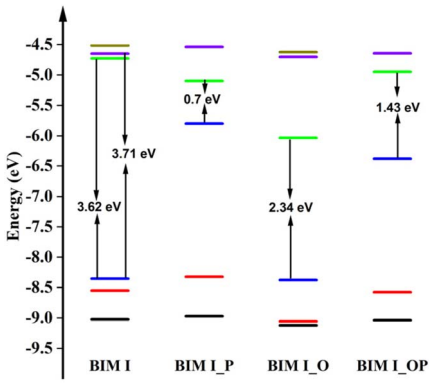


Fig. 8 From left to right: Energy level diagram of (a) BIM I, (b) protonated BIM I, (c) oxidised BIM I, (d) oxidised-protonated BIM I.

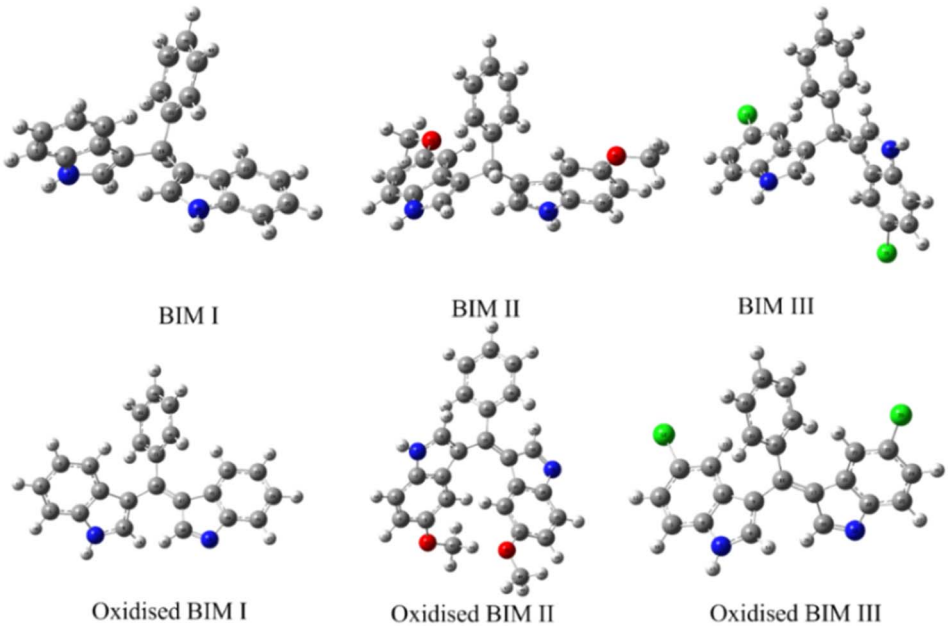


Fig. 7 Optimised ground state geometries of BIM I, BIM II, and BIM III (above) and their oxidised form (below).

in Fig. 8 and S15.† Theoretical calculations of oxidised BIM derivatives strongly suggest the formation of oxidised BIM in an acidic medium. The HOMO → LUMO energy gap of oxidised BIM derivatives come close to the ground state bleach signal that we are getting in acidic methanol. The HOMO of the oxidised BIM derivatives is close to the normal BIM derivatives suggesting a stable oxidised product. LUMO of oxidised BIM derivatives are stabilised as compared to normal form, and due to enhanced conjugation, the electron density on the benzene ring increases in LUMO. The more localised electron density in oxidised BIM suggests the charge transfer within the molecule. The energy level and MO diagrams of all derivatives and their optimised geometries are listed in the ESI.†

Further evidence for the decreased chances for *meso*-H dissociation is obtained from the corresponding bond strength of the C–H vibration (Table ST2†). It can be seen that for the methoxy derivative the C–H bond is stronger in the hypothetical protonated state. In contrast, the bond is weaker for the remaining two derivatives. Now, although the protonated state does not exist in the ground state, its existence in the excited state is not ruled out. It is well known that the excited state acidities are significantly different from those of the ground state. The change in p$K_a$ can be as high as to make a base act as an acid and *vice versa*. It is possible that the BIM derivatives take up the proton in the vicinity, which eventually dissociates to give rise to an oxidised form. The TD-DFT calculations show substantial reorientation of the indole rings around the *meso* carbon (Fig. S16 and Table ST3†) and also reveal that the *meso* C–H bond weakens further in the excited state. The frequency of C–H bond is tabulated in Table ST4† and the optimised energies for all the molecules are tabulated in Table ST5.† It is understood that the role of solvent is crucial in stabilising the excited states. Thus, directly comparing the gas phase calculations and those with solution phase experiments is not ideal. However, the calculations support the weakening of the *meso* C–H bond under acidic conditions, which is the contention drawn based on experimental observations.

So far, the discussion has shown that *meso* H dissociation is enhanced under acidic conditions. In order to ascertain this, an ideal experiment would be to study the photophysics in non-polar aprotic solvent. However, the solubility of BIM derivatives is poor in such solvents (Fig. S17†). So, we have monitored the photophysics in SDS micelles. A recent work on BIM **I** in SDS micelles has shown that it is encapsulated in the micelle and remains in unaggregated form.[32,36,37] In the experiments presented in this work, the SDS concentrations are maintained four times above CMC (1 CMC ~8.2 mM) to ensure molecules are isolated. Such encapsulation results in increased solubility of BIM derivatives, which otherwise have poor solubility in aqueous medium because of aggregation. Further, the protonation of indolic nitrogen is prevented in this fairly non-polar microenvironment. Under these conditions, it is expected that the photoexcitation should not result in the breaking of the C–H bond. Nearly a five-fold enhancement in fluorescence was observed for BIM **I** and BIM **II** beyond the critical micellar concentration, indicating a restricted environment due to encapsulation (Fig. S18†). The BIM **III**, however, did not show similar enhancement. This could be attributed to a relatively higher solubility of BIM **III** in water than the other two derivatives. The transient data give clear evidence of the hindrance to the dissociation of *meso*-hydrogen in surfactant assemblies. The slow decay beyond 10 ps in SDS, post-excitation, is significantly slower for all three molecules (Fig. 9 and S19†). Hence, the slow component can be ascribed to de-excitation due to reorientation. This process is faster in methanolic conditions. However, it is interesting to note that the initial kinetics below 10 ps is the same in SDS, alkaline, and neutral conditions. This is true for all three derivatives. However, the initial kinetics are significantly different under acidic conditions. In the case of BIM **I**, a negative signal in acidic conditions was observed at wavelengths around 500 nm. In SDS micelles, no such negative signal is observed (Fig. 9). Instead, an immediate rise similar to alkaline and neutral conditions is observed. The sub 10 ps kinetics under acidic and micellar medium completely overlap with each other as we move towards the red wavelengths. This

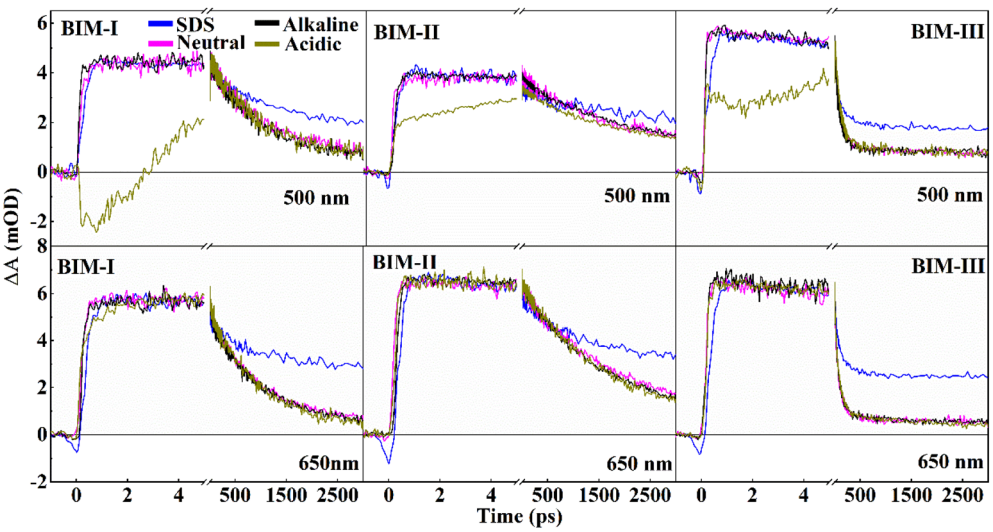


Fig. 9 Kinetic traces at 500 nm and 650 nm of BIM I, BIM II, and BIM III in neutral, alkaline, acidic and SDS micellar medium.

feature is observed in aqueous and alkaline medium as well. BIM **II** and BIM **III** also show similar features where the decays of the ESA are different in acidic conditions, while they are comparable in restricted micellar environments, alkaline and neutral mediums (Fig. S20–S22†). The computational calculations have indicated that the protonation of the indole moiety reduces the HOMO–LUMO gap, which results in the change of colour. Under the restricted non-polar environment provided by the SDS micelles, protonation is prevented, due to which the loss of *meso*-H is also prevented. Hence, it is beyond doubt that the acidic conditions are necessary and play a significant role in controlling the ultrafast dynamics post-excitation.

## Conclusion

The bis(indolyl)methanes show an increased propensity to lose the *meso*-H under acidic conditions. This feature is further amplified when the electron density on the indole rings is reduced. In the presence of bulky electron-donating groups, this propensity is decreased, however, activation by light can trigger the loss of *meso*-proton. The importance of an acidic environment for enhanced cleavage of the *meso* C–H bond was supported through a control experiment in SDS micelles, where cleavage of the *meso* C–H bond was not observed. In SDS micelles, the BIM derivatives are expected to reside inside the micelles, the BIMs do not get protonated and, consequently, do not dissociate. The photophysical investigations on the excited state dynamics of BIM derivatives presented in this work would help design efficient bis(indolyl)methane-based scaffolds for vivid applications.

## Data availability

The data supporting this article have been included as part of the ESI.†

## Author contributions

E. S. S. I. conceptualised and implemented the idea. V. K. J. carried out all the spectroscopic investigations and data analysis. S. K. P. performed quantum chemical calculations. D. C. R. and K. G. synthesised the compounds. All the authors wrote the manuscript.

## Conflicts of interest

There are no conflicts to declare.

## Acknowledgements

V. K. J. and S. K. P. thank IIT Goa for the fellowship. E. S. S. I. thanks the Ministry of Earth Science, Government of India, for a research grant MoES/PAMC/DOM/55/2023 (E-12933). All authors thank IIT Goa and the University of Delhi for providing the research facilities. The authors thank the reviewers for the valuable comments and suggestions.

## References

1 S. Wang, W. X. Ren, J. Hou, M. Won, J. An, X. Chen, J. Shu and J. S. Kim, *Chem. Soc. Rev.*, 2021, **50**, 8887–8902.
2 P. R. Simha, M. S. Mangali, D. K. Gari, P. Venkatapuram and P. Adivireddy, *J. Heterocycl. Chem.*, 2017, **54**, 2717–2724.
3 K. Gopalaiah, S. N. Chandrudu and A. Devi, *Synthesis*, 2015, **47**, 1766–1774.
4 H. Ramshini, B. Mannini, K. Khodayari, A. Ebrahim-Habibi, A. S. Moghaddasi, R. Tayebee and F. Chiti, *Eur. J. Med. Chem.*, 2016, **124**, 361–371.
5 R. J. Sundberg, *The Chemistry of Indoles*, Academic Press, New York 1996.
6 B. Bao, Q. Sun, X. Yao, J. Hong, C. O. Lee, C. J. Sim, K. S. Im and J. H. Jung, *J. Nat. Prod.*, 2005, **68**, 711–715.
7 P. Ertl, S. Jelfs, J. Mehlbacher, A. Schuffenhauer and P. Selzer, *J. Med. Chem.*, 2006, **49**, 4568–4573.
8 T. R. Garbe, M. Kobayashi, N. Shimizu, N. Takesue, M. Ozawa and H. Yukawa, *J. Nat. Prod.*, 2000, **63**, 596–598.
9 M. Shiri, M. A. Zolfigol, H. G. Kruger and Z. Tanbakouchian, *Chem. Rev.*, 2010, **110**, 2250–2293.
10 U. P. Panday and P. Thilagar, *Adv. Opt. Mater.*, 2020, **190**, 2145.
11 N. Seyedi and H. Khabazzadeh, *Res. Chem. Intermed.*, 2015, **41**, 2603–2607.
12 P. J. Praveen, P. S. Parameswaran and M. S. Majik, *Synthesis*, 2015, **47**, 1827–1837.
13 M. Marrelli, X. Catchet, F. Conforti, R. Sirianni, A. Chimento and V. Pezzi, *Nat. Prod. Res.*, 2013, **27**, 2039–2045.
14 X. Tian, K. D. Liu, F. Ma, Z. Li and M. H. Lee, *Cancer Lett.*, 2018, **448**, 20–30.
15 A. A. Panov, S. N. Lavrenov, E. P. Mirchink, E. B. Isakova, A. M. Korolev and A. S. Trenin, *J. Antibiot.*, 2021, **74**, 219–224.
16 S. B. Bharate, J. B. Bharate, S. I. Khan, B. L. Tekwani, M. R. Jacob and R. Mudududulla, *Eur. J. Med. Chem.*, 2013, **63**, 435–443.
17 Y. S. Zhao, H. L. Ruan, X. Y. Wang, C. Chen, P. F. Song and C. W. Lu, *RSC Adv.*, 2019, **9**, 40168–401675.
18 R. C. R. Golcalves, P. Panavaler, S. P. G. Costa, J. C. Morales and M. M. M. Raposo, *Molecules*, 2023, **28**, 7728.
19 S. Sarva, J. S. Harinath, S. P. Sthanikam, S. Ethiraj, M. Vaithiyalingam and S. R. Cirandur, *Chin. Chem. Lett.*, 2016, **27**, 16–20.
20 M. Damodiran, D. Muralidharan and P. T. Perumal, *Bioorg. Med. Chem. Lett.*, 2009, **19**, 3611–3614.
21 C. Grosso, A. L. Cardoso, A. Lemos, J. Varela, M. J. Rodrigues, L. Custodio, L. Barreira and T. Melo, *Eur. J. Med. Chem.*, 2015, **93**, 9–15.
22 K. V. Sashidhara, M. Kumar, R. Sonkar, B. S. Singh, G. Khanna and A. K. Bhatia, *J. Med. Chem.*, 2012, **55**, 2769–2779.
23 D. J. Faulkner, *Nat. Prod. Rep.*, 2001, **18**, 1.
24 S. Imran, M. Taha and N. Ismail, *Curr. Med. Chem.*, 2015, **22**, 4412–4433.
25 E. F. Blanco-Acuna and H. Garcia-Ortega, *J. Mol. Struct.*, 2022, **1265**, 133507.

26 D. Maciejewska, M. Rasztawicka, I. Wolska, E. Aunszewska and B. Gruber, *Eur. J. Med. Chem.*, 2009, **44**, 4136–4147.
27 V. Singh, A. Dogra, J. Das, P. Manna and N. Gupta, *FlatChem*, 2021, **29**, 100279.
28 G. S. S. Kumar, S. Kumaresan, A. A. M. Prabhu, N. Bhuvanes and P. G. Seethalakshmi, *Spectrochim. Acta, Part A*, 2013, **101**, 254–263.
29 N. Azizi, L. Torkian and M. R. Saidi, *J. Mol. Catal. A:Chem.*, 2007, **275**, 109–112.
30 P. S. Tessaro, M. N. Tomaz, G. Farias, C. P. De Paula, M. C. Rocha, I. Malazavi, B. F. Pimenta, H. F. Terenzi, S. R. Mendes, R. A. Gariani and F. R. Xavier, *J. Inorg. Biochem.*, 2022, **236**, 111973.
31 F. Lafzi, H. Killik, B. Ertugrul, M. Arik and N. Saracogulu, *J. Lumin.*, 2018, **208**, 174–182.
32 P. Paul, S. Samanta, B. Mondal, S. K. Saha, U. K. Roy, A. Mallick and T. Majumdar, *ChemNanoMat*, 2024, **10**, 4.
33 M. Gayatri, R. S. Fernandes, R. R. Awasthi, D. Sriram and N. Dey, *J. Mol. Liq.*, 2025, **421**, 126776.
34 M. Gayatri, J. Kumari, A. Gangopadhyay and N. Dey, *J. Mol. Liq.*, 2024, **410**, 125266.
35 P. Paul, S. Samanta, A. Mallick and T. Majumdar, *Chem. Phys. Impact*, 2024, **8**, 100526.
36 P. Paul, S. Samanta, A. Chatterjee, A. Mallick and T. Majumdar, *Phys. Chem. Chem. Phys.*, 2023, **25**, 10166–10174.
37 S. Samanta, P. Paul, A. Chatterjee, U. K. Roy, T. Majumdar and A. Mallick, *Langmuir*, 2024, **40**, 8961–8970.
38 L. Wanga, X. He, Y. Guo, J. Xu and S. Shao, *Lett. Org. Chem.*, 2011, **8**, 60–65.
39 X. He, S. Hu, K. Liu, Y. Guo, J. Xu and S. Shao, *Org. Lett.*, 2006, **8**, 333–336.
40 R. Martínez, A. Espinosa, A. Tárraga and P. Molina, *Tetrahedron*, 2008, **64**, 2184–2219.
41 I. Gryczynski, W. Wiczk, M. L. Johnson and J. R. Lakowicz, *Biophys. Chem.*, 1988, **32**(2–3), 173–185.
42 R. Pegu and S. Pratihar, *ChemistrySelect*, 2016, **1**, 3288–3296.
43 N. K. Kalluvettukuzhy, S. Pagidi, R. P. Nandi and P. Thilagar, *Asian J. Org. Chem.*, 2020, **9**, 644–651.
44 M. Karar, S. Paul, A. Mallick and T. Majumdar, *ChemistrySelect*, 2017, **2**, 2815–2821.
45 A. Neshat, *RSC Adv.*, 2016, **6**, 32839–32848.
46 M. Frisch, G. Trucks, H. Schlegel, G. Scuseria, M. Robb, J. Cheeseman, G. Scalmani, V. Barone, G. Petersson and H. Nakatsuji, *et al.*, *Gaussian 16, Revision C. 01*; Gaussian, Inc.: Wallingford, CT, 2016.
47 J. Tirado-Rives and W. L. Jorgensen, *J. Chem. Theory Comput.*, 2008, **4**, 297–306.
48 L. Lu, H. Hu, H. Hou and B. Wang, *Comput. Theor. Chem.*, 2013, **1015**, 64–67.
49 M. M. Francl, W. J. Pietro, W. J. Hehre, J. S. Binkley and M. S. Gordon, *J. Chem. Phys.*, 1982, **77**, 3654–3665.
50 G. A. Petersson and M. A. AI-Laham, *J. Chem. Phys.*, 1991, **94**, 6081–6090.
51 S. Arulmozhiraja and M. L. Coote, *J. Chem. Theory Comput.*, 2012, **8**, 575–584.
52 J. Peon, G. C. Hess, J. L. Pecourt, T. Yuzawa and B. Kohler, *J. Phys. Chem. A*, 1999, **103**, 2460–2466.
53 B. Albinsson and B. Norden, *J. Phys. Chem.*, 1992, **96**, 6204–6212.
54 J. Al, T. Slanina, E. Palao and P. Klán, *Photochem. Photobiol. Sci.*, 2016, **15**(2), 250–259.
55 S. Jha, N. Kumari, B. Chettri and N. Dey, *ChemPhysChem*, 2022, **23**, e202200208.
56 M. G. D. Nix, A. L. Devine, B. Cronin and M. N. R. Ashfold, *Phys. Chem. Chem. Phys.*, 2006, **8**, 2610–2618.
57 H. Saigusa, *J. Photochem. Photobiol., C*, 2006, **7**, 197–210.
58 R. Montero, Á. P. Conde, V. Ovejas, F. Castaño and A. Longarte, *J. Phys. Chem. A*, 2012, **116**, 2698–2703.
59 J. Peon, J. D. Hoerner and B. Kohler, *ACS Symp. Ser. Am. Chem. Soc.*, 2002, **820**, 122–135.
60 L. Serrano-Andrés and B. O. Roos, *J. Am. Chem. Soc.*, 1996, **118**, 185–195.